ISTITUTO NAZIONALE DI RICERCA METROLOGICA
Repository Istituzionale

Molecular surface coverage standards by reference-free GIXRF supporting SERS and SEIRA substrate benchmarking

(Article begins on next page)

18 January 2025

Research Article

Eleonora Cara*, Philipp Hönicke, Yves Kayser, Burkhard Beckhoff, Andrea M. Giovannozzi,
Petr Klapetek, Alberto Zoccante, Maurizio Cossi, Li-Lin Tay, Luca Boarino and
Federico Ferrarese Lupi

Molecular surface coverage standards by reference-free GIXRF supporting SERS and SEIRA substrate benchmarking

Abstract: Non-destructive reference-free grazing incidence X-ray fluorescence (RF-GIXRF) is proposed as a highly effective analytical technique for extracting molecular arrangement density in self-assembled monolayers. The establishment of surface density standards through RF-GIXRF impacts various applications, from calibrating laboratory XRF setups to expanding its applicability in materials science, particularly in surface coating scenarios with molecular assemblies. Accurate determination of coverage density is crucial for proper functionalization and interaction, such as in assessing the surface concentration of probes on plasmonic nanostructures. However, limited synchrotron radiation access hinders widespread use, prompting the need for molecular surface density standards, especially for benchmarking substrates for surface-enhanced Raman and infrared absorption spectroscopies (SERS and SEIRA) as well as associated surface-enhanced techniques. Using reproducible densities on gold ensures a solid evaluation of the number of molecules contributing to enhanced signals, facilitating comparability across substrates. The research discusses the importance of employing molecular surface density standards for advancing the field of surface-enhanced spectroscopies, encouraging collaborative efforts in protocol development and benchmarking in surface science.

Keywords: self-assembled monolayer; grazing-incidence X-ray fluorescence; SERS SEIRA; molecular surface density; surface coverage standards

1 Introduction

Self-assembled monolayers (SAMs) manifest as highly organized and densely packed two-dimensional molecular arrangements that spontaneously develop on various substrate surfaces through the bottom-up process of self-assembly. One of the crucial parameters to evaluate the quality of the formed self-assembled monolayer is its packing density. The development of characterization methods allowing to measure the efficiency of SAMs formation has a broad impact on various applications.

In fact, the self-assembly approach holds immense potential for generating innovative molecular architectures and has become an integral facet of nanomaterial manufacturing. SAMs have garnered significant attention for their versatile application to surface modifications in various scientific fields. In the realm of chemistry, the molecular assembly technique finds application in the creation of novel supramolecular structures, e.g. modifying the wettability, friction, adhesion, and corrosion resistance, of the substrate material. In the field of biology and medicine, SAMs have demonstrated important tools for the realization of biocompatible surfaces [1], selective immobilization sites for biomolecules [2], [3], and drug delivery systems [4].

*Corresponding author: Eleonora Cara, Istituto Nazionale di Ricerca Metrologica, Torino, Italy, E-mail: e.cara@inrim.it.
https://orcid.org/0000-0002-5981-9569
Philipp Hönicke, X-ray Spectrometry, Physikalisch-Technische Bundesanstalt, Berlin, Germany; and Helmholtz-Zentrum Berlin, Hahn-Meitner Platz 1, 14109 Berlin, Germany
Yves Kayser, X-ray Spectrometry, Physikalisch-Technische Bundesanstalt, Berlin, Germany; and Max Planck Institute for Chemical Energy Conversion, Stiftstr. 34–36, 45470 Mülheim an der Ruhr, Germany
Burkhard Beckhoff, X-ray Spectrometry, Physikalisch-Technische Bundesanstalt, Berlin, Germany
Andrea M. Giovannozzi, **Luca Boarino** and **Federico Ferrarese Lupi**, Istituto Nazionale di Ricerca Metrologica, Torino, Italy
Petr Klapetek, Czech Metrology Institute, Brno, Czech Republic
Alberto Zoccante and **Maurizio Cossi**, Dipartimento di Scienze e Innovazione Tecnologica, Università degli Studi del Piemonte Orientale Amedeo Avogadro Sede di Alessandria, Alessandria, Italy
Li-Lin Tay, NRC, Ottawa, Canada

Analogously, the impact of SAMs in the vast field of nanotechnology is extended to the development of chemically-directed self-assembly as a patterning strategy [5], surface engineering methods for perovskite solar cells efficiency [6], as well as electronic components such as molecular-scale transistors and organic electronic materials [7].

For the aforementioned applicative fields of SAMs, different molecular units can be chosen depending on the desired properties and the substrate material. Thiols constitute a large class of molecules with a sulfur-containing functional group that readily bonds with various metals, including noble metals, creating stable and well-organized monolayers while phosphonic or carboxylic acids are used for the functionalization of other metal and metallic oxide surfaces, including alumina and titania. Silanes and amines are other widely used classes of molecules forming SAMs on silica-based surfaces and other metallic surfaces, such as platinum [7].

The mechanism of SAM formation has been the object of several studies concerning different chemical species and substrate surfaces, to understand the chemical bond as well as the packing mechanism of the molecular units leading to different achievable densities. For a specific molecule, the quality of the SAM improves with tighter packing. The surface coverage of SAMs is particularly vital, as demonstrated in the passivation of surfaces [8] and in the functionalization of sensing platforms, like surface plasmon resonance substrates, where SAMs bind proteins, antibodies, and other biomolecules, influencing immobilization efficiency and offering control over the process [9]. In organic electronics, SAMs are used to tailor the work function between source and drain metal electrodes and to facilitate charge transfer from the metal electrode to the organic semiconductor [10].

The knowledge of the surface coverage of SAMs is relevant to offer precise control over interface properties, enhancing device performance and stability [11]. Alkanedithiols SAMs with engineered backbone lengths have been used to fine-tune the gap distance between plasmonic gold nanoparticles leading to the controllable onset of quantum regime properties [12]. In surface-enhanced spectroscopies, such as surface-enhanced Raman spectroscopy (SERS) [13] and surface-enhanced infrared absorption spectroscopies (SEIRA) [14] a monolayer of molecules adsorbed within the distance invested by enhanced electric field can be used to benchmark the sensor performance for which surface density of the probes is crucial. In the literature, only a few methods have been proposed to determine the density of molecular assemblies, e.g. involving inductively plasma-coupled mass spectrometry [15], electrochemical method [16], [17], and surfactants adsorption isotherm [18].

In the following, we explore a method known as synchrotron-radiation-based X-ray fluorescence under grazing incidence conditions (GIXRF) [19], schematized in Figure 1. In GIXRF, a monochromatic and low-divergent X-ray beam is used at a well-defined shallow angle of incidence which is varied around the critical angle for total external reflection of a flat sample to record the variation of the X-ray fluorescence intensity (Figure 1a). For grazing incidence angles below the critical angle, the interference between the incident and reflected X-ray beam generates an X-ray standing wave (XSW) field just above the sample surface, as shown in Figure 1b, such that the emitted fluorescence from the atoms depends on their position within the XSW. Moreover, the grazing incidence conditions substantially reduce X-ray fluorescence and other background contributions arising from the sample's bulk volume. This technique serves as a non-destructive tool to quantify and depth profile atomic species, relying on the fundamental parameters approach derived from Sherman's equation [20]. In addition, by utilizing physically calibrated X-ray spectrometry instrumentation at the BESSY II synchrotron radiation facility, eliminates the need for a calibration standard or reference sample in the so-called reference-free (RF) approach [21]. This advantage of RF-GIXRF has been already reported for the absolute quantification and depth profiling of doping levels in semiconductors [22]. Due to these attributes, RF-GIXRF proves well-suited for establishing standards applicable to laboratory-based applications and offers a mean to assess the mass density of target atoms on a surface or at a subsurface depth and relate this to the surface density of the molecular species carrying that atom. The identified target atom must be distinguishable from the other elements in the molecular structure or in the substrate and must have atomic number Z higher than 4. Indeed, the target element should be different from the other constituents of organic molecules (C, N, O) and needs to have a detectable characteristic X-ray fluorescence line with well-known atomic fundamental parameters (FPs). RF-GIXRF enables the determination of the molecular surface density of SAMs in an absolute manner, ensuring complete traceability to the international system of units. Considering sulfur as the target element in thiol molecules, the mass of sulfur per unit flat area σ_S (g cm^{-2}) can be determined through Equation (1) from the $S - K\alpha,\beta$ fluorescence count rates $P_{S,K}$ obtained by deconvolving the fluorescence spectra (Figure 1c), measured with a radiometrically calibrated energy-dispersive detector [23].

$$\sigma_S = \frac{1}{k} \cdot \frac{\sin \theta}{\Phi_0 \cdot \Omega/4\pi} \cdot \frac{P_{S,K}}{\varepsilon_{(E_{S,K})} \cdot I_{XSW}(E_0, \theta) \cdot \tau_{S,K}(E_0) \cdot \omega_{S,K}}$$
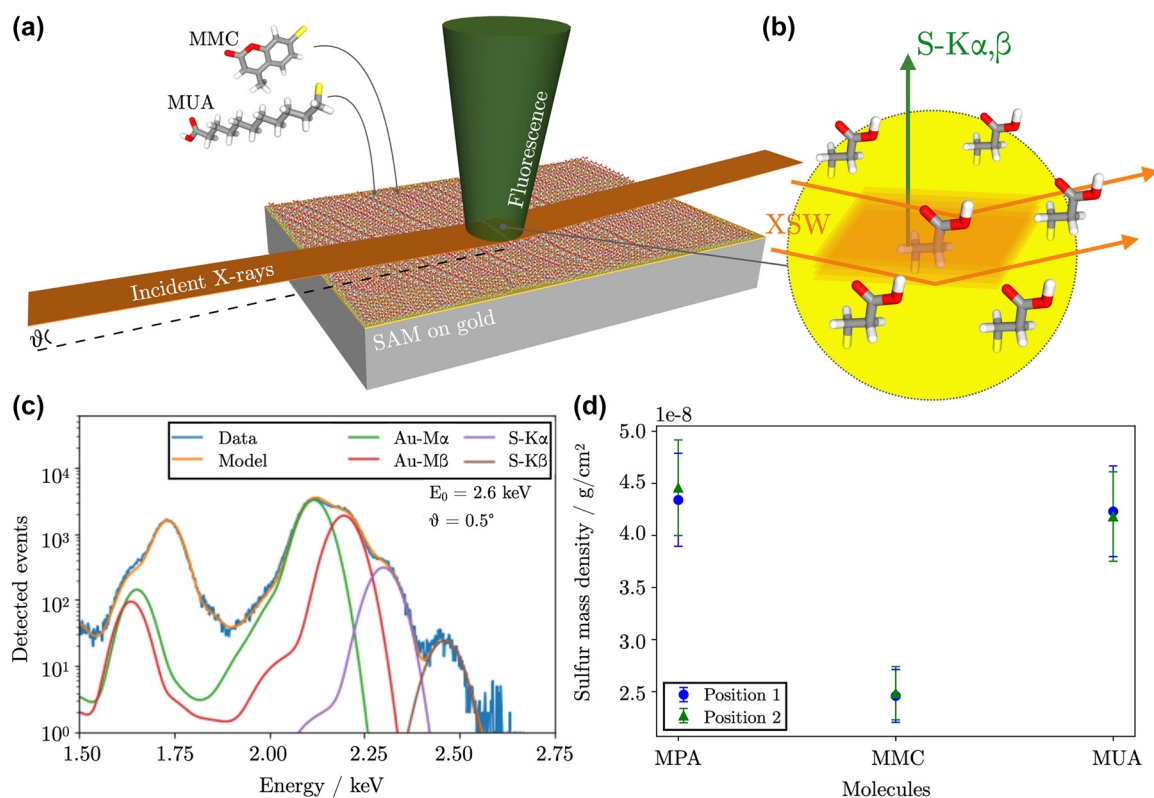
(1)

Figure 1: RF-GIXRF scheme and results. (a) The schematic representation of the gold-coated silicon substrate is reported, with a self-assembled monolayer of MPA molecules. The X-ray beam with energy $E_0 = 2.6$ keV impinges on the surface at varying grazing angles θ. The excited fluorescence radiation, emitted isotropically, is detected above the sample [23]. (b) A close-up scheme shows the presence of the XSW field, responsible for the excitation of X-ray fluorescence of the atoms above the surface. (c) The deconvolved spectrum, recorded at 0.5°, is shown and the derived S − Kα,β count rates are used to calculate the mass density of sulfur. The remaining spectral contributions at about 1.74 keV are due to Si − Kα substrate fluorescence. (d) Scatter plot reporting the sulfur mass density σ_S extracted from two different points on the SAM through RF-GIXRF scanning.

In Equation (1), the FPs accounting for the fluorescence production cross-section, i.e. the partial photoionization cross-section τ and the fluorescence yield ω for sulfur K shell, are combined with calibrated instrumental and experimental parameters, i.e. grazing incidence angle θ, the solid angle of detection $\Omega/4\pi$, incoming photon flux Φ_0, detector efficiency ϵ and angle-dependent intensity of the XSW field. The factor k is the ratio between the effective surface area of the sample and its geometrical area so that $1/k$ accounts for the correct distribution of the target element on the substrate. The molecular surface density μ_{mol} can be easily deduced from the sulfur mass density through Equation (2).

$$\mu_{mol} = \frac{1}{n_S} \cdot \sigma_S \cdot \frac{N_A}{w_S} \qquad (2)$$

where n_S is the number of sulfur atoms per molecule, w_S and N_A are the sulfur atomic weight and Avogadro's number, respectively. The quantification methods can be applied to determine the packing density of organic compounds with sulfhydryl or phosphonic acid anchor groups

by selecting sulfur and phosphorus as the target atoms, respectively, provided they are not present elsewhere in the molecule structure. Additionally, the quantification through RF-GIXRF could be used for other applications and including other molecular systems, e.g. phosphorous-based polypeptoid brush layers used for deterministic doping of semiconductors [24], where P can be identified as target element, as well as a variety of molecules in SAMs used as selective contacts in perovskite solar cells [25], such as 4-bromobenzoic acid or 4-(trifluoromethyl)benzoic acid where the target atoms could be chosen to be bromine or fluorine, respectively.

We previously demonstrated the potential of this analytical method in the determination of the μ_{mol} on complex gold nanostructures used as SERS substrates, exciting the fluorescence at 45° to probe molecules distributed on the 3D nanostructures, and we validated this result with molecular dynamics (MD) simulations finding comparable values for the packing of 7-mercapto-4-methylcoumarin (MMC) as well as comparable enhancement factor values for a

three-dimensional nanostructured SERS substrate derived both experimentally and computationally [26].

In this paper, we report the absolute quantification of the number of molecules per unit area for three SAMs of thiol molecules via RF-GIXRF with full traceability to the international system of units and corroborate these results with molecular dynamics simulations. We discuss a possible application of the derived molecular surface density standards for benchmarking SERS and SEIRA substrates, providing a protocol for utilization of such molecular standards.

2 Results and discussion

2.1 Sample preparation

To establish molecular surface density standards experimentally, we identified three probes. These molecules are 7-methyl-4-mercaptocoumarin (MMC), 3-mercaptopropionic acid (MPA), and 11-mercaptoundecanoic acid (MUA). The quantification of SAMs coverage by RF-GIXRF has been conducted on silicon dies covered with a 100 nm thick gold layer (Figure 1a). The gold surface was scanned by atomic force microscopy (AFM) to determine the k factor in Equation (1), i.e. the ratio between the surface area and the flat projected area, finding a value of $k = (1.0076 \pm 0.0014)$. Consequently, the $1/k$ correction factor in Equation (1) was evaluated as (0.9925 ± 0.0014). Each gold-covered substrate was cleaned with O_2 plasma and incubated for 2 h in an ethanol-based solution at a 0.1 mM concentration of one of the probes and rinsed copiously with ethanol afterward to remove any excess.

2.2 Molecular surface density quantification: experimental and computational approaches

In the RF-GIXRF experiment, spectra were collected at two different regions across the surface of each functionalized sample with areas corresponding to that excited by the X-ray beam footprint. One non-functionalized gold surface served to quantify the sulfur background content resulting from typical air contamination, which persisted despite meticulous handling and O_2 plasma cleaning. This contamination was detected at the techniques's lower sensitivity threshold (few ng/cm^2).

The values of the mass density of sulfur, displayed in Figure 1d, were derived from the sulfur Kα,β photon counts in the XRF spectra on functionalized substrates, and were corrected for background contamination and converted through Equation (2) to the number of molecules

Table 1: Molecular surface density values derived from RF-GIXRF measurements and MD simulations.

	MMC (molecules/nm^2)	MPA (molecules/nm^2)	MUA (molecules/nm^2)
RF-GIXRF	4.1 ± 0.6	7.6 ± 1.1	7.3 ± 1.1
MD	4.2	6.8	7.1

per unit area assembled on the gold surface. The quantification on substrates incubated with 0.1 mM solutions of MMC molecules yielded a μ_{mol} value of (4.1 ± 0.6) molecules per nm^2. The other molecular surface densities are (7.3 ± 1.1) nm^{-2} for MUA, and (7.6 ± 1.1) nm^{-2} for MPA, also summarized in Table 1. These results are comparable within the uncertainties to the MPA density $((6.3 \pm 0.6)$ molecules/nm$^2)$ reported in the work by Hinterwirth et al. for curved nanoparticle surfaces [15]. This suggests that standard values acquired under controlled conditions can be reasonably considered comparable across a range of complex metallic structures. The uncertainties reported are due to the propagation of uncertainties for independent measurements. For each of the tested molecules, the values of the σ_S carry a relative uncertainty of 11 %, due to the single terms in Equation (1) where the largest uncertainty contribution is given by the fluorescence yield ω reported at the denominator [21].

The results from RF-GIXRF measures can be compared with the densest monolayer models obtained by MD simulations, searching for the highest densities that are dynamically stable at the given temperature. A similar approach has been previously used for MMC monolayers [27]. The protonation state of the sulfur atom bonded to the metal is still debated. Some researchers claim that at least in some monolayers it keeps the hydrogen giving rise to a thiol (R-SH) physisorption [28]–[30] although most studies suggest the chemisorption of radical thiyls (R-S) [31]–[34].

To address this, we previously reported the MD simulations of both thiol and thiyl monolayers, to investigate if the maximum dynamically stable densities differ and what agrees better with the spectroscopic data finding a significant predominance of thyil radicals in the SAM [27].

We considered MMC, MPA, and MUA monolayers. In all the cases, more and more thiyls were packed randomly on a flat gold surface, then the system was let to evolve dynamically for a sufficient time to achieve thermal equilibrium. Every system reached a maximum density, above which some thiyls detach from the surface and move to an unbound state floating over the actual monolayer, as visible for MMC in Figure 2. We assume that these molecules would
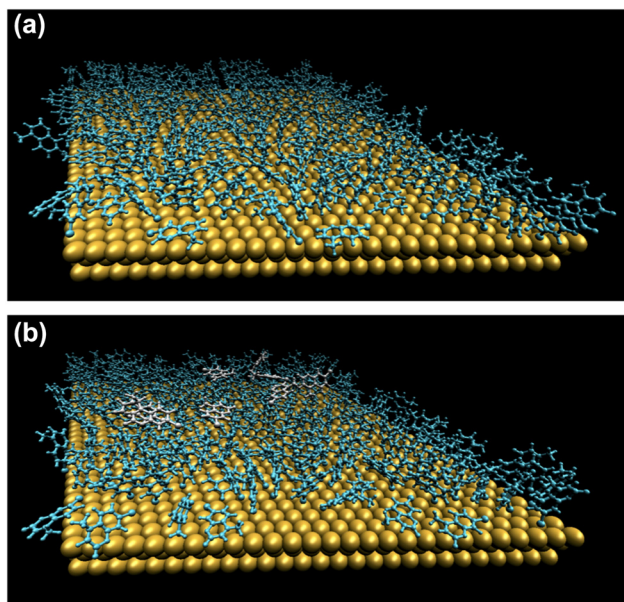
Figure 2: Molecular dynamics simulations. (a) MMC SAM at a density lower than 4.1 molecules/nm^2. All molecules (light blue) remained adjacent to the gold surface during the dynamics. (b) MMC SAM at a density higher than 4.1 molecules/nm^2. Some molecules (white) detached from the gold surface during the dynamics.

be washed away during the synthesis, thus not contributing to the final density. The maximum stable densities reached by all the systems are listed in Table 1. The MD results agree with the RF-GIXRF data within the uncertainty for chemisorbed thiyl radicals.

2.3 Surface coverage standards for SERS and SEIRA substrates benchmarking

The progress of surface-enhanced spectroscopies has been pushed by the development of competitive nano and microstructured plasmonic antennae. The definitive establishment of SERS and SEIRA as trustworthy sensing techniques is bound to the standardization of their methodology as identified as a priority in a recent review [13]. In this view, an important first European interlaboratory comparison has addressed the experimental issues related to accomplishing comparability and reproducibility in SERS quantitative analyses, especially targeting standard methods for sample preparation, data acquisition, and analysis [35]. The evaluation of the performance of the sensors has been largely debated within the scientific community over the years [36]–[38]. The parameters that have been mostly used so far to evaluate and compare the performance of SERS substrates are the enhancement factor (EF) and the limit of detection (LOD) [39], [40].

Concerning the former, the agreed definition for the average EF of a substrate consists in the ratio between the intensities of the SERS/SEIRA signal and reference signal acquired in non-enhanced conditions. These are normalized to the number of molecules N contributing to each of them across the substrate [14], [41]. The number of molecules adsorbed on the plasmonic surface and contributing to the enhanced signal either Raman or infrared absorption, $N_{\text{SERS/SEIRA}}$, depends on the surface concentration of the adsorbates μ_{mol}, the metallic surface area A_M, the density of metallic structures μ_M, and the area A of the excitation due to the incident radiation as reported in Equation (3) [41], [42].

$$N_{\text{SERS/SEIRA}} = A_M \cdot \mu_{\text{mol}} \cdot \mu_M \cdot A \qquad (3)$$

Some critical issues have been identified as open challenges [37], [43], [44], including the orientation of the adsorbates with respect to the metallic surface, their surface density μ_{mol}, and the surface area in complex nanostructures A_M [42]. The number of active molecules weights strongly on the uncertainty associated with the EF [45]. In the evaluation of the absolute EF only the molecules localized inside hot spots are considered because those can actually benefit from the intensified electric field. However, the determination of the hot spot volume is usually pursued through ideal electromagnetic simulation and the current comprehension is that the extent of the hot spots can vary during the measurement, leading to several assumptions for the evaluation of the number of molecules involved. Underestimating (overestimating) $N_{\text{SERS/SEIRA}}$ hinders the realistic evaluation of the EF resulting in exceedingly large (low) values and impeding comparability and reproducibility. As we proved in our earlier study, the SERS EF varies significantly with respect to different number densities of the probe molecule μ_{mol} at the hot spots sites, determined either through geometrical estimations or via synchrotron-radiation-based reference-free X-ray fluorescence measurements [26]. One-to-one comparisons of SERS substrates enhancement capabilities are made possible by adopting the same surface coverage [46], [47] or the same geometrical assumptions [48], [49] for the evaluation of N_{SERS}, provided that the same test molecule is used, as well as other proposed methods for its experimental determination [50]. However, this practice is not commonly adopted in the evaluation of the EF, even when the same probe is utilized. Frequently, disparate density values [51], [52] or varying assumptions regarding molecular occupancy [53], [54] are employed to estimate the number of active molecules.

As emphasized previously [55], choosing standard analytes for benchmarking substrates could overcome this issue. The knowledge of standard values of the adsorbates'

surface density can contribute to the standardization process. Molecular surface densities determined under consistent and reproducible conditions (e.g. planar gold surface) by RF-GIXRF, offer hands-on support and address the need for benchmarking sensors based on surface-enhanced spectroscopies [55]. The molecules selected for the RF-GIXRF experiment are suitable candidates for benchmarking SERS substrates, according to the following criteria: they establish a stable bond with the metallic surface and do not present a strong resonance effect, unlike rhodamine 6G and Raman dyes [55]. These molecules can be adopted for the initial characterization of any substrate with gold nano or microstructures to compare all substrates in a robust manner before moving on to other molecules of interest with unknown adsorption properties for which different metrics, such as LOD, may be more relevant. Hereafter, we discuss the steps, schematized in Figure 3, required to determine $N_{\text{SERS/SEIRA}}$ when standard molecules with known surface densities are selected to benchmark SERS sensors with variegate morphologies. In the formula for $N_{\text{SERS/SEIRA}}$ (also reported in Equation (3)), the metallic surface area

A_M of the nanostructure unit on every specific substrate (Figure 3a) needs to be accurately determined to be able to convert the surface density to a numerical value. Determing A_M constitutes the most challenging task for the determination of N_{SERS} when dealing with substrates with complex morphologies, if the surface coverage is known through the proposed reference values. Atomic force microscopy can serve this purpose on rough structures developing mainly in two dimensions, as in reference [56], [57]. While for 3D structures with dendritic or branched morphology as the one in reference [58], gas adsorption analysis using N_2 for monolayer capacity is more effective to determine the surface area.

After functionalizing the substrates for 2 h of incubation in 0.1 mM ethanol-based solution as detailed in the Experimental section, standard μ_{mol} can be used for the corresponding molecule when these are adsorbed on the rough and nano or microstructured plasmonic surfaces (Figure 3b). It is then required to carefully evaluate the illumination conditions to determine the total number of active nanostructures within the excitation spot through μ_M

$$N_{\text{SERS/SEIRA}} = \underbrace{A_M}_{\text{(a)}} \; \underbrace{\mu_{\text{mol}}}_{\text{(b)}} \; \underbrace{\mu_M \cdot A}_{[26,41]}$$

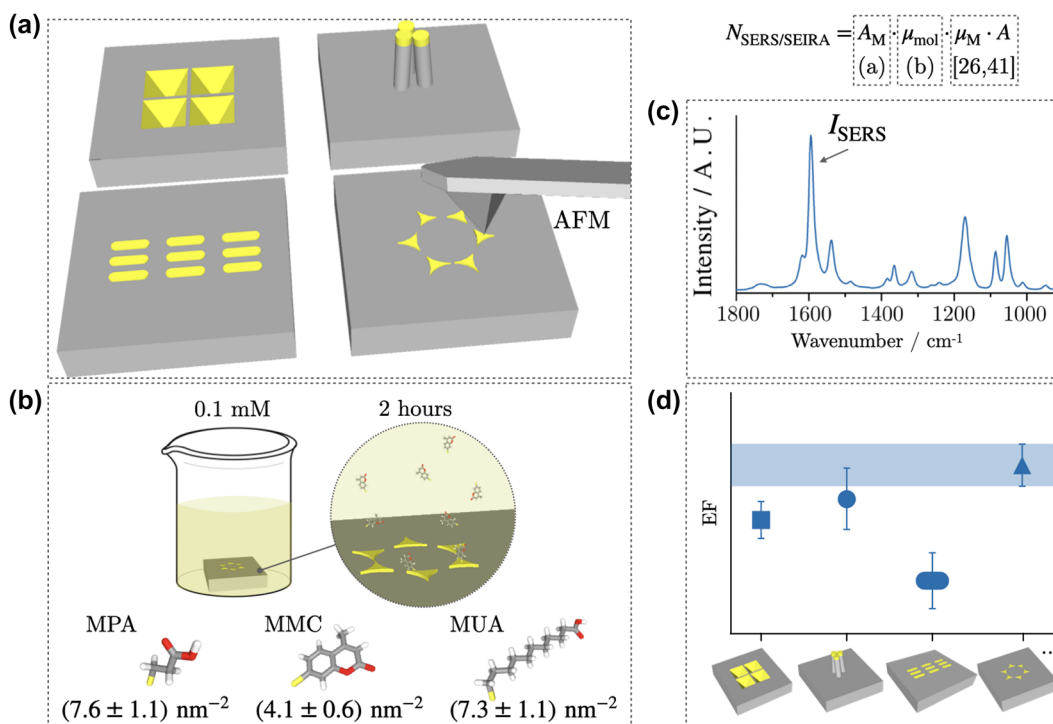MPA (7.6 ± 1.1) nm^{-2} MMC (4.1 ± 0.6) nm^{-2} MUA (7.3 ± 1.1) nm^{-2}

Figure 3: Schematic illustration of the workflow to estimate the $N_{\text{SERS/SEIRA}}$ from the determined standard surface densities and to compare the EFs. (a) For different nanostructures, the determination of the metallic surface area A_M should be done in every specific case and could be evaluated by AFM scans. (b) After the substrate functionalization with 0.1 mM solution of the chosen test molecule for 2 h followed by thorough rinsing, the standard molecular surface density values μ_{mol} (molecules per square nanometer), determined through RF-GIXRF, can be used to benchmark SERS and SEIRA sensors. The μ_M and A factors can be estimated by following references [26], [42]. (c) The enhanced spectrum (here as an example, the SERS spectrum of MMC) is acquired to determine enhanced signal intensity. (d) The values of EF for the different sensors can be reliably compared if the uncertainty associated with each value is reported, as schematically illustrated in the scatter plot where the second substrate would have the highest EF comparable to the third one within the uncertainty.

and *A* according to the methods discussed in previous works [26], [42]. The derived number of molecules should be used to normalize the intensity of the enhanced signals of one or more peaks of the fingerprint spectrum of the molecule (Figure 3c). The normal Raman conditions contributing to the EF should be determined according to the methods discussed in reference [42] while reference conditions in infrared absorption can be determined through the method in reference [14]. Additionally, to be able to compare sensors with different morphologies to one another (Figure 3d), the uncertainty carried by each term in Equation (3) should be considered and the total uncertainty should be presented with the EF, as shown in reference [26].

3 Conclusions

In conclusion, the discussed analytical technique, non-destructive reference-free grazing incidence X-ray fluorescence, proves effective in extracting the density of molecular arrangement in self-assembled monolayers. The establishment of surface density standards is useful in calibrating laboratory XRF setups, thereby extending the applicability of this analytical technique. Additionally, RF-GIXRF plays a significant role across various domains of materials science, particularly in scenarios necessitating surface coating with molecular assemblies. Accurately determining coverage density is essential for ensuring proper functionalization and interaction with tailored molecules or complete passivation. Specifically, this technique allows the determination of surface concentration of probes on plasmonic nanostructures, addressing a critical factor in assessing substrates' performance and enabling meaningful comparison. Limited synchrotron radiation access impedes widespread use of RF-GIXRF, prompting the establishment of molecular surface density standards, specifically measuring thiols on plasmonic metals or other molecules [59] suitable for SERS/SEIRA substrates benchmarking. Using selected molecules with standard densities that can be confidently reproduced on gold contributes to a solid evaluation of $N_{\text{SERS/SEIRA}}$ as long as the surface area of the metallic structures and hot spots locations is accurately determined on each sensor. This guarantees better comparability of enhancement performances on different substrates, in addition to reporting results according to pre-established guidelines or checklists [55], as it happens already for the efficiency of solar conversion devices [60]. Establishing and implementing transferrable protocols for SERS and SEIRA sensors benchmarking using well-characterized molecules is required before moving to unknown analytes for quantification purposes [61]. To this end, additional

international collaborative efforts facilitate discussions to establish appropriate performance metrics and constitute a tangible step toward standardization, including the definition of protocols for signal intensity acquisition. The RF-GIXRF and the analogous grazing-exit XRF method [62] still need to be developed to further characterize SAMs in terms of the molecular orientation with respect to the substrates, which is a relevant quantity for different applications, including organic electronics, SERS, and SEIRA [14].

4 Experimental section

4.1 Materials

The three thiol molecules used for the SAM formation were purchased from Sigma-Aldrich Merck, as well as the gold rods for the thin film evaporation. The silicon wafers were purchased from MEMC, Novara.

4.2 Self-assembled monolayer preparation

A silicon wafer was diced in rectangles of 1×3 cm^2, the shape is necessary to contain the whole X-ray beam footprint incident at grazing angles. Electron-beam evaporation was used to deposit a 100 nm film of gold on the silicon dies, using a typical e-beam current of 70 mA and deposition rate of circa 1 Å/s with a residual pressure of $3 \cdot 10^{-6}$ mbar. A plasma cleaning process was performed in O$_2$ atmosphere at a residual pressure of $7 \cdot 10^{-2}$ mbar at 40 W for 6 min (Plasma Matrix BDiscom) prior to the incubation in the probe solutions. The samples were then immersed for 2 h in 0.1 mM solution of each of the three molecules in ethanol and rinsed thoroughly with ethanol afterward.

4.3 Atomic force microscopy

The AFM used (Bruker Dimension Icon) for the determination of the surface area on the gold substrates was calibrated against an interferometric scanning probe microscope using step height standards to maintain the traceability to the SI. It was equipped with two fresh tips for hard tapping mode (Bruker RTESPA-525) to account for the tip convolution and tip wear. Several scans of the gold surface were carried out on 25 µm^2 areas (2,048 × 2,048 pixels) and optimized to reduce noise and prevent leveling to affect the statistical results [63]. The surface area was evaluated through the statistical analysis tool in Gwyddion open-source software [64]. The uncertainty was evaluated by combining additional measurements in non-ideal

conditions and simulations using synthetic tools in Gwyddion [65], considering the variations across the sample (largest contribution), microscope calibration, feedback loop faults, leveling, tip convolution, and noise.

4.4 Grazing-incidence X-ray fluorescence

The GIXRF experiment took place at the PTB four-crystal monochromator (FCM) beamline [66] at the BESSY II electron storage ring in Berlin, Germany. This beamline is equipped with a four-crystal monochromator (FCM) that allows for adjusting the incident X-ray beam's energy in the range of 1.75 keV – 10.5 keV. To quantify sulfur, a low-divergence monochromatic X-ray beam with a photon energy of $E_0 = 2.6$ keV was employed, exceeding the X-ray absorption edge for sulfur K shell at 2.472 keV. The instrumental setup is installed in an ultra-high vacuum (UHV) chamber [23] and incorporates calibrated photodiodes essential for the alignment procedure and measuring key characteristics of the incoming beam as described in Equation (1). These measurements include a full-width at half maximum beam width of (300 ± 20) µm and a photon flux $\Phi_0 = (4.5 \pm 0.1) \cdot 10^8$ photons per second. The zero-angle motor position (θ_0), where the beam is parallel to the sample surface, was determined for each sample mounted on a motorized stage. This stage allows the necessary controlled movement along three translational axes and one rotational axis, altering the θ angle of incidence between the beam and the sample surface within the range of $0° - 7°$ with increments of $0.5°$.

Fluorescence emitted during the process was detected using a physically calibrated energy-dispersive silicon drift detector (SDD) positioned at 90° with respect to the incident beam. The solid angle of detection $(\Omega/4\pi)$ was equal to 0.005 sr in the angular range of the measurement. Understanding the detector response functions and detection efficiency at different energies facilitates spectral deconvolution and the extraction of detected fluorescence intensities for the S, K fluorescence lines [67]. The strong Au−M peak's proximity had no impact on sulfur peak deconvolution, as adjustments were made for peak height rather than position and shape. This adjustment reduced the degree of freedom, enhancing the reliability of the deconvolution process.

4.5 Molecular dynamics

The MD simulations were performed with the GROMACS software suite, using GROMOS 54A7 force field for all the parameters, except those involving the interactions sulfur/gold which were previously optimized [27]. After an initial energy minimization to remove spurious close contacts,

the constant number of particles, volume and temperature (NVT) MD simulation runs were performed for equilibration (1.0 ns with a 0.5 fs time step), and production (2.0 ns with 1.0 fs time step). A 2 nm cut-off was used for the van der Waals and electrostatic interactions, using the PME method for longer distances. During all the simulations, Au positions were kept frozen.

Author contributions: All authors have accepted responsibility for the entire content of this manuscript and approved its submission.

Conflict of interest: Authors state no conflicts of interest.

Data availability: The datasets generated and/or analysed during the current study are available from the corresponding author upon reasonable request.

References

[1] X. Yuan, *et al.*, "Engineering biocompatible interfaces via combinations of oxide films and organic self-assembled monolayers," *ACS Appl. Mater. Interfaces*, vol. 12, no. 14, p. 17121, 2020.

[2] F. Ghorbanizamani, E. G. Celik, H. Moulahoum, and S. Timur, *Biophysics at the Nanoscale*, Amsterdam, Elsevier, 2024, pp. 1−25.

[3] D. Samanta and A. Sarkar, "Immobilization of bio-macromolecules on self-assembled monolayers: methods and sensor applications," *Chem. Soc. Rev.*, vol. 40, no. 5, p. 2567, 2011.

[4] J. Yang, H.-W. An, and H. Wang, "Self-assembled peptide drug delivery systems," *ACS Appl. Bio Mater.*, vol. 4, no. 1, p. 24, 2020.

[5] K. Tahara, *et al.*, "Self-assembled monolayers as templates for linearly nanopatterned covalent chemical functionalization of graphite and graphene surfaces," *ACS Nano*, vol. 12, no. 11, p. 11520, 2018.

[6] S. Y. Kim, S. J. Cho, S. E. Byeon, X. He, and H. J. Yoon, "Self-assembled monolayers as interface engineering nanomaterials in perovskite solar cells," *Adv. Energy Mater.*, vol. 10, no. 44, p. 2002606, 2020.

[7] M. Singh, N. Kaur, and E. Comini, "The role of self-assembled monolayers in electronic devices," *J. Mater. Chem. C*, vol. 8, no. 12, p. 3938, 2020.

[8] S. Garvey, *et al*., "Effect of alkanethiol chain length on the oxidation resistance of self-assembled monolayer passivated Ge(100) surfaces," *Thin Solid Films*, vol. 778, p. 139875, 2023.

[9] L. Sarcina, *et al*., "Controlling the binding efficiency of surface confined antibodies through the design of mixed self-assembled monolayers," *Adv. Mater. Interfaces*, vol. 10, no. 12, p. 2300017, 2023.

[10] J. Kim, *et al*., "Interface control in organic electronics using mixed monolayers of carboranethiol isomers," *Nano Lett.*, vol. 14, no. 5, p. 2946, 2014.

[11] S. Casalini, C. A. Bortolotti, F. Leonardi, and F. Biscarini, "Self-assembled monolayers in organic electronics," *Chem. Soc. Rev.*, vol. 46, no. 1, p. 40, 2017.

[12] J. Jose, *et al*., "Particle size-dependent onset of the tunneling regime in ideal dimers of gold nanospheres," *ACS Nano*, vol. 16, no. 12, p. 21377, 2022.

[13] J. Langer, *et al*., "Present and future of surface-enhanced Raman scattering," *ACS Nano*, vol. 14, no. 1, pp. 28−117, 2019.

[14] J. Kozuch, K. Ataka, and J. Heberle, "Surface-enhanced infrared absorption spectroscopy," *Nat. Rev. Methods Prim.*, vol. 3, no. 1, p. 70, 2023.

[15] H. Hinterwirth, S. Kappel, T. Waitz, T. Prohaska, W. Lindner, and M. Lämmerhofer, "Quantifying thiol ligand density of self-assembled monolayers on gold nanoparticles by inductively coupled plasma−mass spectrometry," *ACS Nano*, vol. 7, no. 2, p. 1129, 2013.

[16] C. Tseng, A. K. Pennathur, D. Blauth, N. Salazar, and J. M. Dawlaty, "Direct determination of plasmon enhancement factor and penetration depths in surface enhanced IR absorption spectroscopy," *Langmuir*, vol. 39, no. 9, p. 3179, 2023.

[17] M. F. Cardinal, *et al*., "Expanding applications of SERS through versatile nanomaterials engineering," *Chem. Soc. Rev.*, vol. 46, no. 13, p. 3886, 2017.

[18] D. A. Perry, *et al*., "Study of adsorption of aminobenzoic acid isomers on silver nanostructures by surface-enhanced infrared spectroscopy," *J. Phys. Chem. C*, vol. 113, no. 42, p. 18304, 2009.

[19] P. Hönicke, *et al*., "Reference-free grazing incidence x-ray fluorescence and reflectometry as a methodology for independent validation of x-ray reflectometry on ultrathin layer stacks and a depth-dependent characterization," *J. Vac. Sci. Technol. A*, vol. 37, no. 4, 2019.

[20] J. Sherman, "The theoretical derivation of fluorescent X-ray intensities from mixtures," *Spectrochim. Acta*, vol. 7, p. 283, 1955.

[21] B. Beckhoff, "Reference-free X-ray spectrometry based on metrology using synchrotron radiation," *J. Anal. At. Spectrom.*, vol. 23, no. 6, p. 845, 2008.

[22] P. Hönicke, B. Beckhoff, M. Kolbe, D. Giubertoni, J. van den Berg, and G. Pepponi, "Depth profile characterization of ultra shallow junction implants," *Anal. Bioanal. Chem.*, vol. 396, p. 2825, 2010.

[23] J. Lubeck, *et al*., "A novel instrument for quantitative nanoanalytics involving complementary X-ray methodologies," *Rev. Sci. Instrum.*, vol. 84, no. 4, p. 045106, 2013.

[24] V. M. Ospina, *et al*., "Brush layers of bioinspired polypeptoids for deterministic doping of semiconductors," *ACS Appl. Electron. Mater.*, vol. 4, no. 12, pp. 6029−6037, 2022.

[25] C. E. P. Galvis, D. A. G. Ruiz, E. Martínez-Ferrero, and E. Palomares, "Challenges in the design and synthesis of self-assembling molecules as selective contacts in perovskite solar cells," *Chem. Sci.*, no. 15, pp. 1534−1556, 2024.

[26] E. Cara, *et al*., "Towards a traceable enhancement factor in surface-enhanced Raman spectroscopy," *J. Mater. Chem. C*, vol. 8, no. 46, p. 16513, 2020.

[27] D. Marchi, *et al*., "Structure and stability of 7-mercapto-4-methylcoumarin self-assembled monolayers on gold: an experimental and computational analysis," *Phys. Chem. Chem. Phys.*, vol. 24, no. 36, p. 22083, 2022.

[28] C. Vericat, M. Vela, G. Benitez, P. Carro, and R. Salvarezza, "Self-assembled monolayers of thiols and dithiols on gold: new challenges for a well-known system," *Chem. Soc. Rev.*, vol. 39, no. 5, p. 1805, 2010.

[29] L. L. Rouhana, M. D. Moussallem, and J. B. Schlenoff, "Adsorption of short-chain thiols and disulfides onto gold under defined mass transport conditions: coverage, kinetics, and mechanism," *J. Am. Chem. Soc.*, vol. 133, no. 40, p. 16080, 2011.

[30] L. Kankate, A. Turchanin, and A. Golzhauser, "On the release of hydrogen from the S−H groups in the formation of self-assembled monolayers of thiols," *Langmuir*, vol. 25, no. 18, p. 10435, 2009.

[31] M. S. Inkpen, Z.-F. Liu, H. Li, L. M. Campos, J. B. Neaton, and L. Venkataraman, "Non-chemisorbed gold−sulfur binding prevails in self-assembled monolayers," *Nat. Chem.*, vol. 11, no. 4, p. 351, 2019.

[32] I. I. Rzeźnicka, J. Lee, P. Maksymovych, and J. T. Yates, "Nondissociative chemisorption of short chain alkanethiols on Au(111)," *J. Phys. Chem. B*, vol. 109, no. 33, p. 15992, 2005.

[33] M. Hasan, D. Bethell, and M. Brust, "The fate of sulfur-bound hydrogen on formation of self-assembled thiol monolayers on Gold: ^{1}H NMR spectroscopic evidence from solutions of gold clusters," *J. Am. Chem. Soc.*, vol. 124, no. 7, p. 1132, 2002.

[34] R. G. Nuzzo, B. R. Zegarski, and L. H. Dubois, "Fundamental studies of the chemisorption of organosulfur compounds on gold(111). Implications for molecular self-assembly on gold surfaces," *J. Am. Chem. Soc.*, vol. 109, no. 3, p. 733, 1987.

[35] S. Fornasaro, *et al*., "Surface enhanced Raman spectroscopy for quantitative analysis: results of a large-scale European multi-instrument interlaboratory study," *Anal. Chem.*, vol. 92, no. 5, p. 4053, 2020.

[36] M. J. Natan, "Concluding remarks: surface enhanced Raman scattering," *Faraday Discuss.*, vol. 132, p. 321, 2006.

[37] M. D. Porter and J. H. Granger, "Surface-enhanced Raman scattering II: concluding remarks," *Faraday Discuss.*, vol. 205, p. 601, 2017.

[38] S. E. Bell, *et al*., "Towards reliable and quantitative surface-enhanced Raman scattering (SERS): from key parameters to good analytical practice," *Angew. Chem., Int. Ed.*, vol. 59, no. 14, p. 5454, 2020.

[39] V. Vendamani, S. N. Rao, A. P. Pathak, and V. R. Soma, "Silicon nanostructures for molecular sensing: a review," *ACS Appl. Nano Mater.*, vol. 5, no. 4, p. 4550, 2022.

[40] E. C. Le Ru and B. Auguié, "Enhancement factors: a central conceptduring 50 years of surface-enhanced Raman spectroscopy," *ACS Nano*, vol. 18, no. 14, pp. 9773−9783, 2024.

[41] E. Le Ru, E. Blackie, M. Meyer, and P. G. Etchegoin, "Surface enhanced Raman scattering enhancement factors: a comprehensive study," *J. Phys. Chem. C*, vol. 111, no. 37, p. 13794, 2007.

[42] E. Le Ru, M. Meyer, E. Blackie, and P. Etchegoin, "Advanced aspects of electromagnetic SERS enhancement factors at a hot spot," *J. Raman Spectrosc.*, vol. 39, no. 9, p. 1127, 2008.

[43] A. I. Pérez-Jiménez, D. Lyu, Z. Lu, G. Liu, and B. Ren, "Surface-enhanced Raman spectroscopy: benefits, trade-offs and future developments," *Chem. Sci.*, vol. 11, no. 18, p. 4563, 2020.

[44] E. C. Le Ru and P. G. Etchegoin, "Quantifying SERS enhancements," *MRS Bull.*, vol. 38, no. 8, p. 631, 2013.

[45] E. C. Le Ru, *et al*., "A scheme for detecting every single target molecule with surface-enhanced Raman spectroscopy," *Nano Lett.*, vol. 11, no. 11, p. 5013, 2011.

[46] M. Hoffmann, S. Wackerow, A. Abdolvand, and S. A. Zolotovskaya, "High performance SERS platforms via parametric optimization of the laser-assisted photodeposition of silver and gold nanoparticles," *Opt. Mater. Express*, vol. 11, no. 9, p. 3079, 2021.

[47] J.-F. Bryche, *et al*., "Density effect of gold nanodisks on the SERS intensity for a highly sensitive detection of chemical molecules," *J. Mater. Sci.*, vol. 50, p. 6601, 2015.

[48] M. S. Schmidt, J. Hubner, and A. Boisen, "Nanopillars: large area fabrication of leaning silicon nanopillars for surface enhanced Raman spectroscopy," *Adv. Mater.*, vol. 24, no. 10, p. 11, 2012.

[49] N. Félidj, *et al*., "Controlling the optical response of regular arrays of gold particles for surface-enhanced Raman scattering," *Phys. Rev. B*, vol. 65, no. 7, p. 075419, 2002.

[50] R. Rastogi, M. Beggiato, E. A. Dogbe Foli, R. Vincent, C. Dupont-Gillain, P. M. Adam, and S. Krishnamoorthy, "Quantifying analyte surface densities and their distribution with respect to electromagnetic hot spots in plasmon-enhanced spectroscopic biosensors," *J. Phys. Chem. C*, vol. 125, no. 18, pp. 9866−9874, 2021.

[51] J.-G. Fan and Y.-P. Zhao, "Gold-coated nanorod arrays as highly sensitive substrates for surface-enhanced Raman spectroscopy," *Langmuir*, vol. 24, no. 24, p. 14172, 2008.

[52] E. S. Babich, *et al*., "Self-assembled silver nanoparticles in glass microstructured by poling for SERS application," *Curr. Appl. Phys.*, vol. 19, no. 10, p. 1088, 2019.

[53] S. He, J. Chua, E. K. M. Tan, and J. C. Y. Kah, "Optimizing the SERS enhancement of a facile gold nanostar immobilized paper-based SERS substrate," *RSC Adv.*, vol. 7, no. 27, p. 16264, 2017.

[54] F. A. Harraz, A. A. Ismail, S. Bouzid, S. Al-Sayari, A. Al-Hajry, and M. Al-Assiri, "Surface-enhanced Raman scattering (SERS)-active substrates from silver plated-porous silicon for detection of crystal violet," *Appl. Surf. Sci.*, vol. 331, p. 241, 2015.

[55] J.-F. Masson, "The need for benchmarking surface-enhanced Raman scattering (SERS) sensors," *ACS Sens.*, vol. 6, no. 11, pp. 3822−3823, 2021.

[56] B. Zou, C. Niu, M. Ma, L. Zhao, and Y. Wang, "Magnetic assembly route to construct reproducible and recyclable SERS substrate," *Nanoscale Res. Lett.*, vol. 14, pp. 1−10, 2019.

[57] V. Dzhagan, *et al*., "Self-organized SERS substrates with efficient analyte enrichment in the hot spots," *ACS Omega*, vol. 9, no. 4, pp. 4819−4830, 2024.

[58] N. A. M. Yussuf, J. Li, Y. J. Jung, and H. Huang, "Design of high SERS sensitive substrates based on branched Ti nanorods," *Sci. Rep.*, vol. 12, no. 1, p. 11631, 2022.

[59] P. Dietrich, *et al*., "Quantification of silane molecules on oxidized silicon: are there options for a traceable and absolute determination?," *Anal. Chem.*, vol. 87, no. 19, p. 10117, 2015.

[60] J. A. Christians, J. S. Manser, and P. V. Kamat, "Best practices in perovskite solar cell efficiency measurements. Avoiding the error of making bad cells look good," *The Journal of Physical Chemistry Letters*, vol. 6, no. 5, pp. 852−857, 2015.

[61] L. Mandrile, A. M. Giovannozzi, A. Sacco, G. Martra, and A. M. Rossi, "Flexible and transparent substrates based on gold nanoparticles and TiO2 for in situ bioanalysis by surface-enhanced Raman spectroscopy," *Biosensors*, vol. 9, no. 4, p. 145, 2019.

[62] P. Hönicke, *et al*., "Simultaneous dimensional and analytical characterization of ordered nanostructures," *Small*, vol. 18, no. 6, p. 2105776, 2022.

[63] D. Nečas, M. Valtr, and P. Klapetek, "How levelling and scan line corrections ruin roughness measurement and how to prevent it," *Sci. Rep.*, vol. 10, no. 1, p. 15294, 2020.

[64] D. Nečas and P. Klapetek, "Gwyddion: an open-source software for SPM data analysis," *Open Phys.*, vol. 10, no. 1, p. 181, 2012.

[65] D. Nečas and P. Klapetek, "Synthetic data in quantitative scanning probe microscopy," *Nanomaterials*, vol. 11, no. 7, p. 1746, 2021.

[66] M. Krumrey and G. Ulm, "High-accuracy detector calibration at the PTB four-crystal monochromator beamline," *Nucl. Instrum. Methods Phys. Res. Sect. A Accel. Spectrom. Detect. Assoc. Equip.*, vol. 467, p. 1175, 2001.

[67] F. Scholze and M. Procop, "Modelling the response function of energy dispersive X-ray spectrometers with silicon detectors," *X-Ray Spectrom. Int. J.*, vol. 38, no. 4, p. 312, 2009.